squares fitting to the temperature-dependent conductivities in Fig. 1b. The 0%, 1% and 3% materials exhibit linear logσ versus $1/T$ plots, and are well described by an Arrhenius expression. Fitting such an expression to the data for these compositions gives activation energies of 55, 83 and 70 kJ mol^{-1} respectively. An Arrhenius expression may also be used to describe the 5% doped material, although the use of a Vogel–Tamman–Fulcher (VTF) expression $\sigma = \sigma_0 T^{-1/2}\exp(-B/(T - T_0))$ gives a slightly better fit. When we take into account the fact that the VTF expression involves a 50% increase in the number of variables used to fit the conductivity data, compared with the Arrhenius expression, the improvement of the fit is marginal. The onset of such a marginal curvature at 5% is exactly what is expected for a composition on the border between region A and region B, and hence is further confirmation of the doping mechanism. With increasing LiTFSI content in region B the logσ versus $1/T$ plots become more curved, and can only be described by a VTF equation. These trends reinforce the interpretation that region A is dominated by conduction in a doped crystalline material. In parallel with the discovery of ionic conductivity in the crystalline polymer:salt complexes, developments are taking place in the ionic conductivity of plastic crystalline materials[15,16]. Although different, the role of defects in conduction is important in both these classes of ionic conductors.

We have demonstrated that it is possible to raise the conductivity of crystalline polymer electrolyte by isovalent doping, and we anticipate that variations of this strategy may lead to other dopants and yet higher conductivity. □

Methods

Samples of PEO_6:$(LiAsF_6)_{1-x}(LiTFSI)_x$ were prepared by dissolving appropriate quantities of $LiAsF_6$ (ABCR, 99.8%), LiTFSI (3M) and –OCH_3 terminated poly(ethylene oxide) with an average molar mass of 1,000 (Fluka, ≥99.5%) together in dry acetonitrile (Aldrich, 99.8%). All constituents were dried before use, and all manipulations were carried out in a high-integrity argon-filled MBraun glove box. After dissolution, the solutions were transferred into glass vials and the solvent allowed to evaporate slowly. The resulting complexes were dried at room temperature under dynamic vacuum for at least 24 h. DSC was carried out using a Netzch DSC 204 Phoenix with heating and cooling rates of 5° min^{-1}.

Powder X-ray diffraction data were collected at room temperature, in transmission mode, using a STOE STADI/P diffractometer with Cu $K_{\alpha 1}$ radiation and a position-sensitive detector. The polymer electrolyte samples were sealed inside glass capillaries, and data were collected with a step size of 0.02° in 2θ.

For conductivity measurements, a sample of each complex was pressed at room temperature between two 0.025-mm-thick stainless-steel disks. These self-supporting disks were placed into two-electrode cells that were, in turn, sealed inside argon-filled cans for removal from the glove box. Each can was placed into an oil bath equipped with a Haake EK30 cooler and a Haake DL30 temperature controller connected to a PC. All internal cell temperatures were monitored using K-type thermocouples also connected to the PC. Conductivity data were obtained using a.c. impedance measurements carried out with a Solartron 1255 frequency response analyser coupled with a Solartron 1286 electrochemical interface. A perturbation voltage of 10 mV was applied over the frequency range 500 kHz–1 Hz. All instruments were connected to the PC, so that the temperature sweep and each a.c. impedance measurement were driven by custom software. Before measurements were made at each temperature, a 2-h equilibration period was enforced after the internal cell temperature of each cell had reached a steady state.

Received 27 September; accepted 11 November 2004; doi:10.1038/nature03186.

1. Scrosati, B. (ed.) *Applications of Electroactive Polymers* (Chapman & Hall, London, 1993).
2. Bruce, P. G. *Solid State Electrochemistry* (Cambridge Univ. Press, Cambridge, 1995).
3. Gray, F. M. *Polymer Electrolytes* (RSC Materials Monographs, The Royal Society of Chemistry, Cambridge, 1997).
4. Tarascon, J.-M. & Armand, M. Issues and challenges facing rechargeable lithium batteries. *Nature* **414,** 359–367 (2001).
5. Barnes, A. *et al.* Towards a 'smart window' for microwave applications. *Smart Mater. Struct.* **7,** 752–758 (1998).
6. Gadjourova, Z., Andreev, Y. G., Tunstall, D. P. & Bruce, P. G. Ionic conductivity in crystalline polymer electrolytes. *Nature* **412,** 520–523 (2001).
7. Stoeva, Z., Martin-Litas, I., Staunton, E., Andreev, Y. G. & Bruce, P. G. Ionic conductivity in the crystalline polymer electrolytes PEO_6:$LiXF_6$, X = P, As, Sb. *J. Am. Chem. Soc.* **125,** 4619–4626 (2003).
8. Shahi, K. & Wagner, J. B. Jr. Fast ion transport in silver halide solid solutions and multiphase mixtures. *Appl. Phys. Lett.* **37,** 757–759 (1980).
9. Ratner, M. A. in *Polymer Electrolytes Reviews – 1* (eds MacCallum, J. R. & Vincent, C. A.) 173–236 (Elsevier Applied Science, London, 1987).
10. Berthier, C. *et al.* Microscopic investigation of ionic conductivity in alkali metal salts – poly(ethylene oxide) adducts. *Solid State Ionics* **11,** 91–95 (1983).
11. Ratner, M. A. & Shriver, D. F. Ion-transport in solvent-free polymers. *Chem. Rev.* **88,** 109–124 (1988).
12. Angell, C. A., Liu, C. & Sanchez, E. Rubbery solid electrolytes with dominant cationic transport and high ambient conductivity. *Nature* **362,** 137–139 (1993).
13. Gadjourova, Z., Martin y Marero, D., Andersen, K. H., Andreev, Y. G. & Bruce, P. G. Structures of the polymer electrolyte complexes PEO_6:LiXF6 (X = P,Sb), determined from neutron powder diffraction data. *Chem. Mater.* **13,** 1282–1285 (2001).
14. Sylla, S., Sanchez, J.-Y. & Armand, M. Electrochemical study of linear and crosslinked POE-based polymer electrolytes. *Electrochim. Acta* **37,** 1699–1701 (1992).
15. MacFarlane, D. R., Huang, J. H. & Forsyth, M. Lithium-doped plastic crystal electrolytes exhibiting fast ion conduction for secondary batteries. *Nature* **402,** 792–794 (1999).
16. Forsyth, M., Huang, J. & MacFarlane, D. R. Lithium doped N-methyl-N-ethylpyrrolidinium bis(trifluoromethanesulfonyl) amide fast-ion conducting plastic crystals. *J. Mater. Chem.* **10,** 2259–2265 (2000).

Acknowledgements P.G.B. is indebted to The Royal Society, the EU and the EPSRC for financial support.

Competing interests statement The authors declare that they have no competing financial interests.

Correspondence and requests for materials should be addressed to P.G.B. (p.g.bruce@st-and.ac.uk).

Rapid stepwise onset of Antarctic glaciation and deeper calcite compensation in the Pacific Ocean

Helen K. Coxall*[1], Paul A. Wilson[1], Heiko Pälike*[2], Caroline H. Lear*[3] & Jan Backman[2]

[1]*Southampton Oceanography Centre, School of Ocean and Earth Science, European Way, Southampton SO14 3ZH, UK*
[2]*Geology and Geochemistry, University of Stockholm, S-10691 Stockholm, Sweden*
[3]*Institute of Marine and Coastal Sciences, Rutgers University, 71 Dudley Road, New Brunswick, New Jersey 08901 USA*

* Present addresses: Graduate School of Oceanography, University of Rhode Island, Bay Campus, South Ferry Rd, Narragansett, Rhode Island 02882, USA (H.K.C.); Southampton Oceanography Centre, School of Ocean and Earth Science, European Way, Southampton SO14 3ZH, UK (H.P.); School of Earth, Ocean and Planetary Sciences, PO Box 914, Cardiff University, Cardiff CF10 3YE, UK (C.H.L.).

The ocean depth at which the rate of calcium carbonate input from surface waters equals the rate of dissolution is termed the calcite compensation depth. At present, this depth is ~4,500 m, with some variation between and within ocean basins. The calcite compensation depth is linked to ocean acidity, which is in turn linked to atmospheric carbon dioxide concentrations and hence global climate[1]. Geological records of changes in the calcite compensation depth show a prominent deepening of more than 1 km near the Eocene/Oligocene boundary (~34 million years ago)[2] when significant permanent ice sheets first appeared on Antarctica[3–6], but the relationship between these two events is poorly understood. Here we present ocean sediment records of calcium carbonate content as well as carbon and oxygen isotopic compositions from the tropical Pacific Ocean that cover the Eocene/Oligocene boundary. We find that the deepening of the calcite compensation depth was more rapid than previously documented and occurred in two jumps of about 40,000 years each, synchronous with the stepwise onset of Antarctic ice-sheet growth. The glaciation was initiated, after climatic preconditioning[7], by an interval when the Earth's orbit of the Sun favoured cool summers. The changes in oxygen-isotope composition across the Eocene/Oligocene boundary are too large to be explained by Antarctic ice-sheet growth alone and must therefore also indicate contemporaneous global cooling and/or Northern Hemisphere glaciation.

The pattern of post-Eocene climate change revealed by benthic $\delta^{18}O$ records is one of abrupt (<1 million year, Myr) increases, superimposed on longer-term $\delta^{18}O$ increases reflecting a combination of global cooling and ice growth[3–6]. Most prominent of the abrupt increases is 'Oi-1' near the Eocene/Oligocene boundary[3–6]. Oi-1 is thought to mark the initiation of major permanent Cenozoic ice-sheets on Antarctica but its cause is widely debated. One hypothesis is that Oi-1 was triggered by the opening of Southern Ocean gateways[3]; another is that it was caused by a threshold response to long-term Cenozoic decline in atmospheric carbon dioxide levels[7]. The Eocene/Oligocene transition also shows a marked calcite compensation depth (CCD) increase in classic Deep Sea Drilling Project (DSDP) records (Fig. 1 inset). However, the timing and duration of CCD increase, the amplitude and implied ice budget of Oi-1 and the relationship between these two events are poorly constrained. Most DSDP and Ocean Drilling Program (ODP) sites spanning the Eocene/Oligocene boundary are afflicted by condensation horizons and hiatuses attributed to increases in ocean circulation vigour and glacioeustatic sea-level fall associated with Antarctic ice-sheet growth[3–5]. Thus, previous interpretations of this key interval are heavily based on records from a handful of mid- to high-latitude sites, none of which are complete, or from the Pacific—the world's largest ocean.

ODP Leg 199 recovered multiple Eocene/Oligocene boundary sections in the tropical Pacific Ocean with unprecedented magneto- and cyclostratigraphic age control[8]. The Eocene/Oligocene transition is instantly recognizable in these strata by up-section shifts from opal-rich to carbonate-rich sediments. We have developed a new chronology for these sections, based on detailed correlation of geological data to astronomically calculated variations of Earth's orbit and solar insolation (ref. 9; the new astronomical solution is available from http://www.imcce.fr/Equipes/ASD/insola/earth/earth.html). ODP Site 1218 provides the best record across the Eocene/Oligocene boundary. To reconstruct CCD changes we determined bulk weight per cent $CaCO_3$ and $CaCO_3$ mass accumulation rate (MAR) by direct measurement on discrete samples and by regression from whole-core analyses of physical properties (Fig. 1). $CaCO_3$ MAR dominates bulk sediment MAR and our records show strong variations on orbital timescales. The sharp increase in $CaCO_3$ around 34 Myr ago (Fig. 1), and the correlative appearance of $CaCO_3$ in deeper water sites[8], suggest that the classic DSDP record (Fig. 1 inset) accurately captures the magnitude of the Eocene/Oligocene CCD increase (≥1 km) in the Pacific Ocean. But the classic DSDP record does not constrain the timing and duration of the shift to better than a 2–3-Myr interval[2], and subsequent studies suggest that it occurred gradually (over several million years)[5,10]. Our new data show that CCD increase took place an order of magnitude faster than this in the Pacific and not as a single event but in two steps (~40 kyr each) separated by an intermediate plateau (~200 kyr, Fig. 1).

To investigate the cause of Eocene/Oligocene CCD increase and its relation to changes in global climate and carbon cycling, we

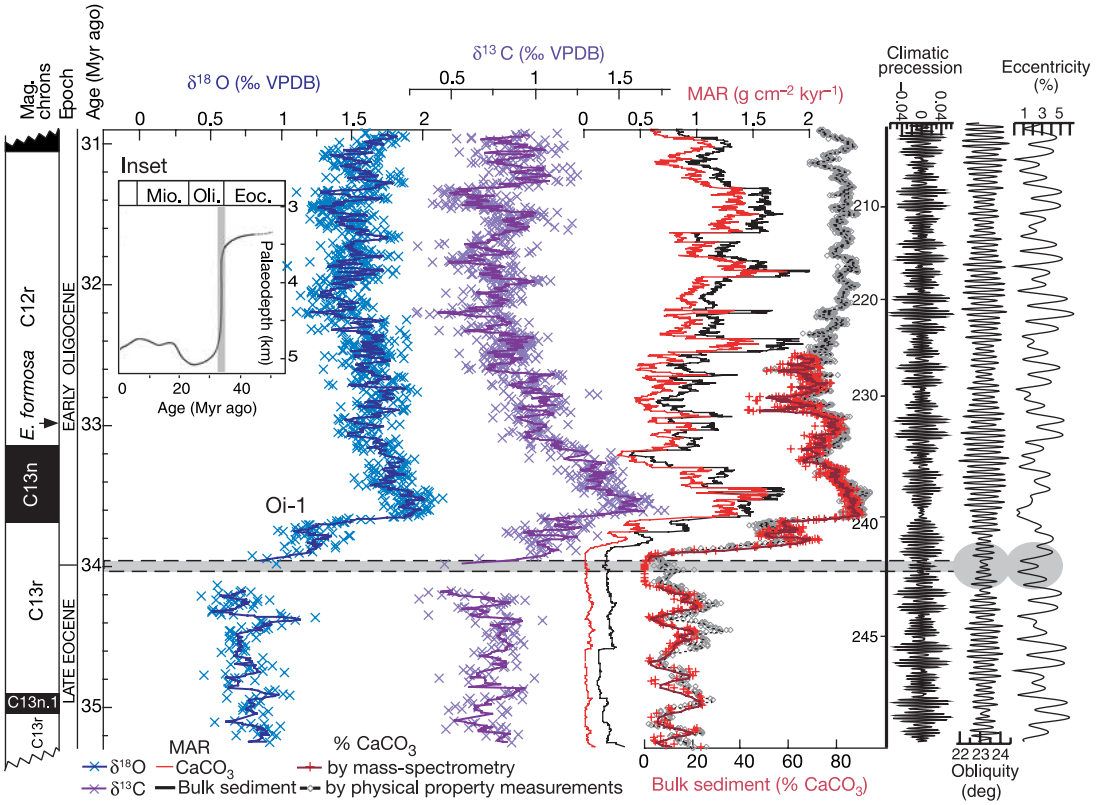

Figure 1 Palaeoceanographic records showing changes in global climate and ocean chemistry for the Eocene/Oligocene transition. The inset shows published[2] CCD for the equatorial Pacific Ocean 50 Myr ago to the present, from classic Deep Sea Drilling Project sites. This published record shows a 1-km deepening near the Eocene/Oligocene boundary but the timing and duration of this shift is poorly constrained (shading = uncertainty of ~3 Myr). The main figure shows new high-resolution data (~35.5 to 31.5 Myr ago) from ODP site 1218 (8° 53.38′ N; 135° 22.00′ W, water depth = 4,862 m; 34 Myr ago palaeolatitude ~0 to 2° N; palaeodepth ≈ 3,800 m), showing that CCD increase (increase in $CaCO_3$) occurred (1) faster than previously documented; (2) in two 40-kyr steps, (3) synchronously with the stepwise onset of major permanent Cenozoic Antarctic ice-sheets ($\delta^{18}O$ increase in benthic foraminiferal calcite) and (4) during an eccentricity minimum and low-amplitude obliquity change (grey shading) favouring cool summers. Benthic $\delta^{13}C$ also shows a stepwise increase. $\delta^{18}O$ = blue; $\delta^{13}C$ = purple; $CaCO_3$=red.

analysed $\delta^{18}O$ and $\delta^{13}C$ in benthic foraminifera (Fig. 1). Our records show that increases in $\delta^{18}O$ and $\delta^{13}C$ documented in mid- and high-latitude South Atlantic[5] and Southern Ocean[11] sites also occur in the Pacific, confirming that these are truly global signals with stratigraphic utility. The contemporaneous occurrence of ice-rafted debris, and a shift from clay mineral assemblages dominated by smectite to those dominated by illite and chlorite in the Southern Ocean, suggest that the first major permanent Cenozoic ice sheets appeared on Antarctica in the early Oligocene[11,12]. Our new records are of the highest resolution (up to 2 kyr) yet achieved for this interval and shed new light on this important event.

Our isotope records show pronounced increases in $\delta^{18}O$ and $\delta^{13}C$ that are synchronous with CCD increase, demonstrating that the transition from a relatively deglaciated climate state in the latest Eocene to a climate state with well-developed ice sheets on Antarctica in earliest Oligocene time was completed within 300 kyr (Fig. 1). Remarkably, the pattern of isotopic increase has the same distinctive stepwise form as our $\%CaCO_3$ series, with most of the $\delta^{13}C$ and $\delta^{18}O$ shift taking place in two 40-kyr-long 'steps'. The two-step Eocene/Oligocene transition in $\delta^{18}O$ occurs in lock-step with that in $CaCO_3$ MAR, but the two-step increase in $\delta^{13}C$ appears to occur slightly later (a $<$10 kyr lag). Furthermore, $\delta^{13}C$, $\delta^{18}O$ and $CaCO_3$ MAR all show a distinctive 'overshoot' of typical early Oligocene values during their earliest Oligocene maxima (Fig. 1). The initiation of step-change in our records occurs during an interval of low eccentricity and low-amplitude change in obliquity, conditions favouring dampened seasonality (Fig. 1). This observation is consistent with the view[7] that it was the prolonged absence of warm summers, inhibiting summer snow melt, not the occurrence of cool winters favouring accumulation, that was important for establishing the first major Cenozoic ice sheets on Antarctica.

The apparent contradiction between our findings and the increased seasonality seen across the Eocene/Oligocene boundary in fish otolith records[13] probably reflects the lack of otolith data from the transition interval of low seasonality because our records demonstrate that, once the Antarctic ice sheet was established, Early Oligocene global climate was highly sensitive to increasing power (seasonality) in the astronomical series (Fig. 1). In other words, the otolith study documents the effect of Antarctic glaciation, whereas our data document its cause. Cross-spectral analyses of our two Oligocene isotope series (~33.25 to 31 Myr ago) show a phase lag of $\delta^{18}O$ with respect to $\delta^{13}C$ corresponding to about 8 kyr in the 40-kyr band (Fig. 2), suggesting that the response of the global carbon cycle to Earth's obliquity helped to force changes in early Oligocene climate.

Our data indicate that Earth's orbital configuration was the ultimate trigger for Oi-1 and the pacemaker for ice-sheet growth. Yet some other conditioning factor must have been important, because there is no evidence to suggest that the low-eccentricity obliquity 'node' conditions at 34 Myr ago are more extreme than those occurring every 2.4 Myr (the eccentricity minimum) and 1.2 Myr (the obliquity minimum) during the past 40 Myr, and

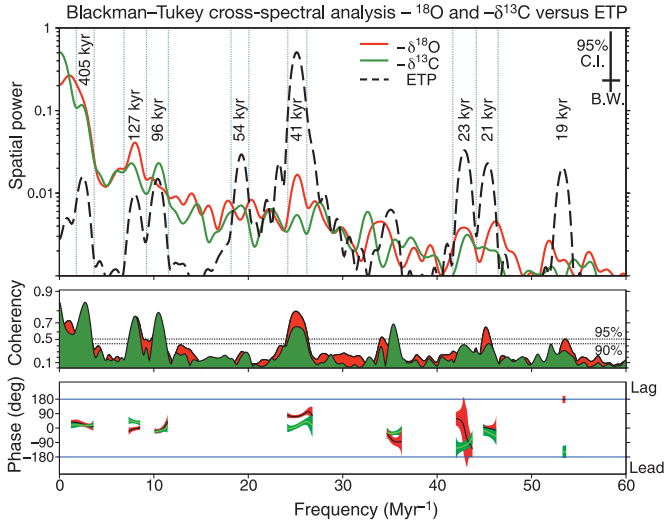

Figure 2 Spectral analysis of ODP site 1218 benthic stable isotopes $\delta^{18}O$ = red; $\delta^{13}C$ = green) and astronomical solution[9] (black dashed line). All astronomical frequencies are encoded within the two Oligocene isotope series, with power concentrated at obliquity ($\delta^{18}O$) and 400-kyr eccentricity ($\delta^{13}C$) frequencies. Cross-spectral analyses indicate that both isotope series are coherent with eccentricity and obliquity above the 95% confidence level, and with elements of climatic precession between the 90% to 95% confidence level. Error bars indicate 95% confidence levels of phase estimates. ETP = mix of eccentricity, tilt (obliquity) and climatic precession, adjusted to simulate the strong eccentricity signal in our data. The phase relationship between the strong obliquity component of the $\delta^{18}O$ data and the weaker component in the $\delta^{13}C$ data suggests a lag of ~8 kyr of $\delta^{18}O$ in the ~40-kyr band (at the ~25 Myr^{-1} frequency). For the high-amplitude 405 kyr and ~100 kyr eccentricity peaks there is no phase difference between the isotope series. B.W., band width.

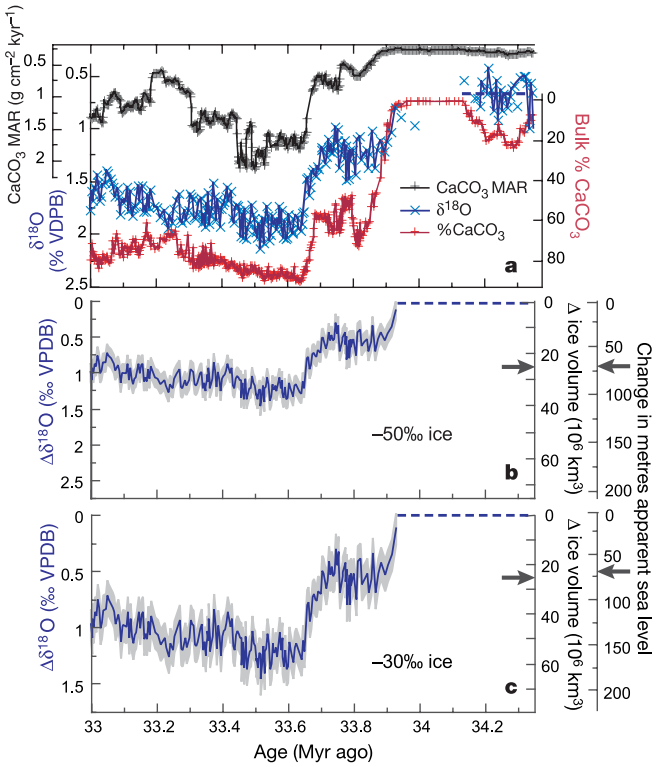

Figure 3 ODP site 1218 records expanded from Fig. 1 and implications of the large $\delta^{18}O$ increase. **a**, Eocene/Oligocene records of $\delta^{18}O$ and CCD ($\%CaCO_3$ and $CaCO_3$ MAR) from Fig. 1. Dashed blue line shows 'base line' mean benthic $\delta^{18}O$ for latest Eocene time (last 400 kyr). **b**, **c**, The early Oligocene increase in $\delta^{18}O$ relative to this baseline ($\Delta\delta^{18}O$) and associated estimated change in global ice budget and metres apparent sea level[17] (m ASL) assuming all of $\Delta\delta^{18}O$ is attributable to increased ice volume (as suggested by Mg/Ca records, see text). Blue, best estimate; grey, estimated uncertainty for sea level change associated with one standard deviation about the Eocene base line. Panel **b** assumes, conservatively, an isotopic composition of Oligocene ice equal to the average for the Antarctic today (−50‰). Panel **c** assumes Oligocene ice is −30‰ (see text). Arrows indicate modern Antarctic ice volume (~25.4 × 10^6 km^3) and ASL fall (70 m) estimated[17] for the Eocene/Oligocene transition by sequence stratigraphy.

possibly back to 50 Myr ago[9,14]. Results of a recent global climate model (GCM) experiment[7] suggest that this conditioning factor was a long-term decline in Cenozoic atmospheric CO_2 levels (Eocene/Oligocene ice-sheet threshold ~2.8 to 3 times the pre-anthropogenic value). In fact, the sudden jumps in ice volume implied by the steps in our $\delta^{18}O$ data are strikingly similar in form to, but three times larger than, those simulated in ref. 7. The steps in the $\delta^{18}O$ data substantiate model predictions[7] of a rapid, non-steady mode of ice-sheet growth in response to mass-balance feedback effects associated with ice-sheet height and coalescence.

Two main factors explain the large amplitude of Oi-1 in our data (1.5 ± 0.1‰) relative to that modelled (~0.5‰)[7]. First, the model considers only Antarctic ice sheets and these are constrained by the coastline, whereas our data reflect continental ice sheets globally and these may expand by seaward advance over newly exposed continental shelf in response to glacioeustatic sea-level fall (grounding line advance). Second, the model considers only ice volume-driven $\delta^{18}O$ increase, whereas our data may incorporate an additional temperature component (cooling). Eocene/Oligocene records of Mg/Ca in deep-sea foraminifera indicate no cooling, which suggests[6,15,16], controversially[13], that all of the $\delta^{18}O$ increase is attributable to ice growth. In Fig. 3 we use our $\delta^{18}O$ data from the central Pacific as a globally representative record to test this suggestion by calculating implied global ice volumes.

Assuming, conservatively, that no pH/$[CO_3^{2-}]$ effect associated with CCD increase acts to suppress $\delta^{18}O$ increase across the Eocene/Oligocene transition and that the average isotopic composition of Antarctic ice was as extreme as today (−50‰) we calculate a global Early Oligocene ice-volume maximum and apparent sea-level[17] (ASL) fall that are about 1.6 times both the modern total Antarctic ice budget (25.4×10^6 km^3) (ref. 18) and the sequence stratigraphic estimate for Eocene/Oligocene ASL fall (70 m) (ref. 17) (Fig. 3b). This calculated Eocene/Oligocene ice volume is similar to that estimated for the maximum extent Last Glacial Maximum on Antarctica (where most of the increase relative to today was achieved by grounding-line advance to near the shelf-slope break all around the continent)[19].

If, in response to a lower latitudinal temperature gradient, we assume that the average isotopic composition of Oligocene Antarctic ice was less extreme than today's (−30‰), the implied global ice budget and ASL fall for the Eocene/Oligocene are correspondingly greater (~2.7 times, Fig. 3c), and impossibly large for Antarctica alone, given its combined continent and shelf area and the limits imposed on ice-sheet thickness by the strong dependence of ice flow on stress[19,20]. These observations raise the possibility of contemporaneous Northern Hemisphere glaciation, consistent with evidence[21] for early onset of North Atlantic Deep Water formation. In any case, our calculated ice volumes are so large that we conclude that Oi-1 must include some cooling component. This would imply that something acts to mask the cooling signal in the Mg/Ca records, possibly the effect of increasing sea-water pH and/or $[CO_3^{2-}]$ associated with CCD increase on Mg partitioning into foraminiferal calcite[16].

Our data show that the Eocene/Oligocene CCD shift was synchronous with the development of major permanent Cenozoic Antarctic ice sheets. Calcite preservation on the sea floor depends on the saturation state of the deep ocean, the flux of organic carbon (C_{org}) to the sea floor and the ratio of this flux to the flux of $CaCO_3$ (refs 1, 22–24). Today, the increase in deep-sea $[CO_3^{2-}]$ associated with a 1-km deepening of the global lysocline yields a drawdown in atmospheric CO_2 of less than 25 μatm (refs 23, 24). Thus, CCD increase is unlikely to have triggered Antarctic glaciation. More probably, glaciation triggered the CCD shift. In fact, the CCD probably deepened to compensate for a reduction in the global ratio of $CaCO_3$ to C_{org} burial, as suggested by the $\delta^{13}C$ increase in benthic foraminiferal calcite (Fig. 1).

It seems improbable that the mechanism responsible was enhanced global Ca^{2+} and CO_3^{2-} flux to the oceans, prompted by glacial weathering[25–27]. Arguably, the most attractive way to explain the apparent teleconnection between the onset of Antarctic glaciation and CCD increase in the tropical Pacific is a shift of global $CaCO_3$ sedimentation from shelf to deep ocean basins[25,28,29]. On 10–20-kyr timescales, the ocean is near saturation with respect to $CaCO_3$, such that any reduction in global shelf and reef carbonate sedimentation will promote increased ocean alkalinity, CCD increase and increased deep-ocean carbonate accumulation. Glacioeustatic sea-level fall associated with the growth of large Antarctic ice sheets would have reduced the size of the shelf carbonate reservoir, promoting higher deep-ocean $[CO_3^{2-}]$ and a deeper CCD. It would also have exposed widespread Upper Cretaceous and Lower Palaeogene limestones to erosion, thereby increasing global river inputs (and $\delta^{13}C$) of dissolved inorganic carbon and alkalinity, further increasing $[CO_3^{2-}]$, deepening the CCD and increasing seawater $\delta^{13}C$ (Fig. 1).

Another mechanism with the potential to contribute to Eocene/Oligocene CCD increase is an increase in global siliceous (at the expense of calcareous) plankton export production[30]. The steady-state response to such a change in $CaCO_3$ export flux (assuming constant river inputs) is likely to be an increase in ocean pH, $[CO_3^{2-}]$ and the depth of the CCD. The power of these (and other) hypotheses to explain the link between Eocene/Oligocene Antarctic glaciation and so rapid, pronounced and permanent a CCD shift needs to be tested using a range of modelling techniques. □

Methods

Chronology

The basis for our new chronology is lithological proxy measurements (bulk density, colour reflectance and magnetic susceptibility) that were collected during ODP Leg 199 using the multi-sensor track (MST) core scanner[8]. We used the MST data, together with additional bulk $\delta^{13}C$, $\delta^{18}O$ and $\%CaCO_3$ measurements from sites 1218 and 1219, to generate an aligned and stacked revised composite depth scale between sites 1218 and 1219. This allowed us to verify the completeness of sediment recovery, as well as the detailed cross-correlation of magnetic reversal and biostratigraphic events. Magnetochron C12n was identified in both sites 1218 and 1219. Chron C13n was recovered in site 1219 only but, by matching characteristic features between holes and sites, our detailed composite depth scale allowed us to constrain the position of C13n within site 1218 on a decimetre scale. Additional shipboard wire-line logging data from site 1218 confirm that the sediment recovered across the Eocene/Oligocene transition is representative of the *in situ* formation, including the double-step and the intervening 'plateau' across this transition in site 1218.

The MST proxy measurements, which in the Oligocene primarily reflect variations of $\%CaCO_3$, allowed us to generate a high-resolution stacked record of $\%CaCO_3$ from the MST data by regression with the bulk measurements. Throughout the Oligocene, these data show remarkably strong variations on orbital eccentricity timescales (~110-kyr and 400-kyr periods), as suggested by the initial, low-resolution, shipboard timescale. The detailed chronology was generated by matching the benthic stable-isotope data from site 1218 with an astronomical template[9]. Our final age model was generated by first matching very clear ~400-kyr and ~110-kyr cycles in the stable-isotope data to the astronomical template, and fine-adjusting individual obliquity (~40 kyr) and climatic precession scale (~22-kyr) cycles throughout the record. The ~400-kyr eccentricity cycle is also present in the colour reflectance data, and was used to constrain the timescale in the upper part of the Eocene, where $\%CaCO_3$ was very low. Amplitude variation of obliquity cycles in the $\delta^{18}O$ record agrees with a ~1.2-Myr cycle in astronomically calculated Earth's obliquity, providing further constraints. Our chronology results in revised estimates for the ages of magnetic reversals between magnetochrons C12n and C13n and the age estimate for the Eocene/Oligocene boundary (Supplementary Information).

$CaCO_3$ data

Bulk sediment $\%CaCO_3$ was measured in small (5–30 mg) discrete samples (3-cm spacing) using both standard high-precision colometric methods and a new rapid-throughput continuous-flow mass-spectrometry technique. These data were also used to calibrate our proxy estimate 'calculated $\%CaCO_3$', determined from a stacked record of whole-core sediment physical properties (gamma-ray attenuation and porosity estimate; magnetic susceptibility; lightness).

Stable-isotope data

We analysed $\delta^{13}C$ and $\delta^{18}O$ in well-preserved *Cibicidoides* benthic foraminifera that are believed to have lived on or just within the sediment–water interface. These were picked from a narrow size fraction (250–400 μm). Because of large inter-sample species abundance fluctuations we analysed a consistent mix of three species (two each of *C. havanensis*, *C. grimsdalei* and *C. subspiratus*). Samples were cleaned ultrasonically and analysed at the Southampton Oceanography Centre using a Europa Geo 20-20 mass

spectrometer equipped with a automatic carbonate preparation system (CAPS). Results are reported relative to the Vienna Pee Dee Belemnite standard (VPDB). Standard external analytical precision, based on replicate analysis of in-house standards calibrated to NBS-19, is better than 0.1‰ for $\delta^{18}O$ and $\delta^{13}C$.

Received 1 September; accepted 25 October 2004; doi:10.1038/nature03135.

1. Broecker, W. S. & Peng, T.-H. The role of $CaCO_3$ compensation in the glacial to interglacial atmospheric CO_2 change. *Glob. Biogeochem. Cycles* **1,** 15–29 (1987).
2. Van Andel, T. H. Mesozoic/Cenozoic calcite compensation depth and the global distribution of calcareous sediments. *Earth Planet. Sci. Lett.* **26,** 187–194 (1975).
3. Kennett, J. P. & Shackleton, N. J. Oxygen isotopic evidence for the development of the psychrosphere 38 Myr ago. *Nature* **260,** 513–515 (1976).
4. Miller, K. G., Wright, J. D. & Fairbanks, R. G. Unlocking the ice house: Oligocene-Miocene oxygen isotopes, eustasy, and margin erosion. *J. Geophys. Res.* **96,** B4, 6829–6849 (1991).
5. Zachos, J. C., Quinn, T. M. & Salamy, K. A. High-resolution (10^4 years) deep-sea foraminiferal stable isotope records of the Eocene-Oligocene climate transition. *Palaeoceanography* **11,** 251–266 (1996).
6. Lear, C. H., Elderfield, H. & Wilson, P. A. Cenozoic deep-sea temperatures and global ice volumes from Mg/Ca in benthic foraminiferal calcite. *Science* **287,** 269–272 (2000).
7. DeConto, R. M. & Pollard, D. Rapid Cenozoic glaciation of Antarctica triggered by declining atmospheric CO_2. *Nature* **421,** 245–249 (2003).
8. Shipboard Scientific Party 2002. Leg 199 summary. *Proc. ODP Init. Rep.* (eds Lyle, M. W., Wilson, P. A. & Janecek, T. R.) **199**, 1–87 (2002).
9. Laskar, J. *et al.* Long term evolution and chaotic diffusion of the insolation quantities of Mars. *Icarus* **170,** 343–364 (2004).
10. Peterson, L. C. Backman, J. Late Cenozoic carbonate accumulation and the history of the carbonate compensation depth in the western equatorial Indian Ocean. *Proc. ODP Sci. Res.* (eds Duncan, R. A., Backman, J., Dunbar, R. B. & Peterson, L. C.) **115**, 467–489 (1990).
11. Salamy, K. A. & Zachos, J. C. Latest Eocene-Early Oligocene climate change and Southern Ocean fertility: inferences from sediment accumulation and stable isotope data. *Palaeogeogr. Palaeoclimatol. Palaeoecol.* **145,** 61–77 (1999).
12. Ehrmann, W. U. & Mackensen, A. Sedimentological evidence for the formation of an East Antarctic ice sheet in Eocene/Oligocene time. *Palaeogeogr. Palaeoclimatol. Palaeoecol.* **93,** 85–112 (1992).
13. Ivany, L. C., Patterson, W. P. & Lohmann, K. C. Cooler winters as a possible cause of mass extinction at the Eocene/Oligocene boundary. *Nature* **407,** 887–890 (2000).
14. Pälike, H., Laskar, J. & Shackleton, N. J. Geologic constraints on the chaotic diffusion of the solar system. *Geology* **32** (11), 929–932 doi: 10.1130/G20750 (2004).
15. Billups, K. & Schrag, D. P. Application of benthic foraminiferal Mg/Ca ratios to questions of Cenozoic climate change. *Earth Planet. Sci. Lett.* **209,** 181–195 (2003).
16. Lear, C. H., Rosenthal, Y., Coxall, H. K. & Wilson, P. A. Late Eocene to early Miocene ice-sheet dynamics and the global carbon cycle. *Paleoceanography* **19,** doi:10.1029/2004PA001039 (2004).
17. Pekar, S. F., Christie-Blick, N., Kominz, M. A. & Miller, K. G. Calibration between eustatic estimates from backstripping and oxygen isotopic records for the Oligocene. *Geology* **30,** 903–906 (2002).
18. Lythe, M. B., Vaughan, D. G. & BEDMAP Consortium, BEDMAP: A new ice thickness and subglacial topographic model of Antarctica. *J. Geophys. Res.* **106,** B6, 11335–11351 (2001).
19. Huybrechts, P. Sea-level changes at the LGM from ice-dynamic reconstructions of the Greenland and Antarctic ice sheets during the glacial cycles. *Quat. Sci. Rev.* **21,** 203–231 (2002).
20. Hindmarsh, R. C. A. Time-scales and degrees of freedom operating in the evolution of continental ice-sheets. *Trans. R. Soc. Edinb. Earth Sci.* **81,** 371–384 (1990).
21. Davies, R., Cartwright, J., Pike, J. & Line, C. Early Oligocene initiation of North Atlantic deep water formation. *Nature* **410,** 917–920 (2001).
22. Archer, D. & Maier-Reimer, E. Effect of deep-sea sedimentary calcite preservation on atmospheric CO_2 concentration. *Nature* **367,** 260–263 (1994).
23. Sigman, D. M. & Boyle, E. A. Glacial/interglacial variations in atmospheric carbon dioxide. *Nature* **407,** 859–869 (2000).
24. Zeebe, R. E. & Westbroek, P. A simple model for the $CaCO_3$ saturation state of the ocean: The "Strangelove," the "Neritan," and the "Cretan" Ocean. *Geochem. Geophys. Geosyst.* **4,** 1104 (2003).
25. Kump, L. R. & Arthur, M. A. in *Tectonics Uplift and Climate Change* (ed. Ruddiman, W. F.) 399–426 (Plenum, New York, 1997).
26. Zachos, J. C., Opdyke, B. N., Quinn, T. M., Jones, C. E. & Halliday, A. N. Early Cenozoic glaciation, Antarctic weathering and seawater $^{87}Sr/^{86}Sr$; is there a link? *Chem. Geol.* **161,** 165–180 (1999).
27. Ravizza, G. & Peucker-Ehrenbrink, B. The marine $^{187}Os/^{188}Os$ record of the Eocene-Oligocene transition: the interplay of weathering and glaciation. *Earth Planet. Sci. Lett.* **210,** 151–165 (2003).
28. Berger, W. H. & Winterer, E. L. in *Plate Stratigraphy and the Fluctuating Carbonate line in Pelagic Sediments: On Land and Under the Sea* (eds Hsü, K. J. & Jenkyns, H. C.) 11–48 (Int. Assoc. Sedimentologists Spec. Publ. 1, Blackwell Science, Oxford, 1974).
29. Opdyke, B. N. & Wilkinson, B. H. Surface area control of shallow cratonic to deep marine carbonate accumulation. *Paleoceanography* **3,** 685–703 (1989).
30. Harrison, K. G. Role of increased marine silica input on paleo-pCO_2 levels. *Paleoceanography* **15,** 292–298 (2000).

Supplementary Information accompanies the paper on **www.nature.com/nature**.

Acknowledgements We thank the Shipboard Party of Ocean Drilling Program Leg 199 for assistance at sea and M. Bolshaw, M. Cooper and H. Birch for laboratory assistance. This work was supported by a NERC UK ODP grant to P.A.W., a Royal Commission for the Exhibition of 1851 fellowship awarded to H.K.C. and by Swedish Research Council (VR) funding to H.P. We thank W. Broecker, R. Hindmarsh, S. D'Hondt, A. Merico, Y. Rosenthal, R. Rickaby, J. Shepherd and T. Tyrrell for discussions and comments on an earlier draft and L. Kump for a constructive review.

Competing interests statement The authors declare that they have no competing financial interests.

Correspondence and requests for materials should be addressed to P.A.W. (paw1@soc.soton.ac.uk).

Similar response of labile and resistant soil organic matter pools to changes in temperature

Changming Fang[1], Pete Smith[1], John B. Moncrieff[2] & Jo U. Smith[1]

[1]*School of Biological Sciences, University of Aberdeen, Aberdeen AB24 3UU, UK*
[2]*Ecology and Resource Management, School of GeoSciences, The University of Edinburgh, Edinburgh EH9 3JU, UK*

Our understanding of the relationship between the decomposition of soil organic matter (SOM) and soil temperature affects our predictions of the impact of climate change on soil-stored carbon[1]. One current opinion is that the decomposition of soil labile carbon is sensitive to temperature variation whereas resistant components are insensitive[2–4]. The resistant carbon or organic matter in mineral soil is then assumed to be unresponsive to global warming[2,4]. But the global pattern and magnitude of the predicted future soil carbon stock will mainly rely on the temperature sensitivity of these resistant carbon pools. To investigate this sensitivity, we have incubated soils under changing temperature. Here we report that SOM decomposition or soil basal respiration rate was significantly affected by changes in SOM components associated with soil depth, sampling method and incubation time. We find, however, that the temperature sensitivity for SOM decomposition was not affected, suggesting that the temperature sensitivity for resistant organic matter pools does not differ significantly from that of labile pools, and that both types of SOM will therefore respond similarly to global warming.

The temperature sensitivity of SOM decomposition, commonly referred to as Q_{10}, is critical for modelling changes in soil C stock[3–6]. The assumption that the decomposition of old organic matter[2–3] or organic C in mineral soil[4] does not vary with temperature—that is, that the decomposition of labile C pools are sensitive, but resistant pools are insensitive, to temperature perturbations—suggests that higher losses of carbon will occur from soils in boreal and tundra regions in response to global warming. This is because these soils have the largest store of labile organic matter, and are predicted to experience the greatest rise in temperature[7]. Tropical soils may release less C than previously predicted[4] owing to a large store of SOM in deep soil[8] and the high proportion of resistant C pools in SOM. Soil warming experiments, an analogue for the effects of global warming on SOM decomposition[9], suggest that the effect of warming on SOM decomposition may decline with time. The change in SOM composition associated with warming and the different temperature sensitivity of the C pools were assumed to be responsible for this decline[10–11]. Despite the common assertion that SOM composition affects the temperature sensitivity of SOM decomposition, experimental or modelling evidence is yet to be presented. If the temperature sensitivity of SOM decomposition is not affected by SOM composition, predictions of climate change impacts on soil stored C will be greatly affected.

By definition, the temperature sensitivity of SOM decomposition is the change in SOM decomposition rate with temperature under otherwise constant conditions[5]. At present, this concept is often confused with concepts of SOM turnover[4,12–13] or SOM dynamics[2–4] under different environmental conditions with accompanying different temperatures. Temperature sensitivity of SOM decomposition (or Q_{10}) estimated by incubating soils at different but constant temperatures[14–16] or by radiocarbon accumulation in undisturbed soils[13] is confounded by many factors other than temperature.

We incubated soil samples under changing temperature to